ANTIOXIDANTS & REDOX SIGNALING
Volume 23, Number 13, 2015
DOI: 10.1089/ars.2015.6297

ORIGINAL RESEARCH COMMUNICATION

Preferential Extracellular Generation of the Active Parkinsonian Toxin MPP^+ by Transporter-Independent Export of the Intermediate $MPDP^+$

Stefan Schildknecht,[1,*] Regina Pape,[1,*] Johannes Meiser,[2] Christiaan Karreman,[1] Tobias Strittmatter,[3] Meike Odermatt,[1] Erica Cirri,[1] Anke Friemel,[3] Markus Ringwald,[4] Noemi Pasquarelli,[5] Boris Ferger,[5] Thomas Brunner,[1] Andreas Marx,[3] Heiko M. Möller,[6] Karsten Hiller,[2] and Marcel Leist[1]

Abstract

Aims: 1-Methyl-4-phenyl-tetrahydropyridine (MPTP) is among the most widely used neurotoxins for inducing experimental parkinsonism. MPTP causes parkinsonian symptoms in mice, primates, and humans by killing a subpopulation of dopaminergic neurons. Extrapolations of data obtained using MPTP-based parkinsonism models to human disease are common; however, the precise mechanism by which MPTP is converted into its active neurotoxic metabolite, 1-methyl-4-phenyl-pyridinium (MPP^+), has not been fully elucidated. In this study, we aimed to address two unanswered questions related to MPTP toxicology: (1) Why are MPTP-converting astrocytes largely spared from toxicity? (2) How does MPP^+ reach the extracellular space? ***Results:*** In MPTP-treated astrocytes, we discovered that the membrane-impermeable MPP^+, which is generally assumed to be formed inside astrocytes, is almost exclusively detected outside of these cells. Instead of a transporter-mediated export, we found that the intermediate, 1-methyl-4-phenyl-2,3-dihydropyridinium ($MPDP^+$), and/or its uncharged conjugate base passively diffused across cell membranes and that MPP^+ was formed predominately by the extracellular oxidation of $MPDP^+$ into MPP^+. This nonenzymatic extracellular conversion of $MPDP^+$ was promoted by O_2, a more alkaline pH, and dopamine autoxidation products. ***Innovation and Conclusion:*** Our data indicate that MPTP metabolism is compartmentalized between intracellular and extracellular environments, explain the absence of toxicity in MPTP-converting astrocytes, and provide a rationale for the preferential formation of MPP^+ in the extracellular space. The mechanism of transporter-independent extracellular MPP^+ formation described here indicates that extracellular genesis of MPP^+ from MPDP is a necessary prerequisite for the selective uptake of this toxin by catecholaminergic neurons. *Antioxid. Redox Signal.* 23, 1001–1016.

Introduction

THE EXPERIMENTAL STUDY of dopamine (DA) neuron degeneration (a hallmark of Parkinson's disease) relies on toxicants that specifically induce pathological states reminiscent of human parkinsonism by inducing the selective death of DA neurons. Among the chemical tools currently used to induce DA neuron degeneration, MPTP (1-methyl-4-phenyl-1,2,3,6-tetrahydropyridine) most closely reproduces human parkinsonian pathology in mice and primates (3, 31).

[1]Department of Biology, University of Konstanz, Konstanz, Germany.
[2]Metabolomics Junior Research Group, Luxembourg Centre for Systems Biomedicine, University of Luxembourg, Esch-Belval, Luxembourg.
[3]Department of Chemistry and Konstanz Research School Chemical Biology, University of Konstanz, Konstanz, Germany.
[4]MCAT GmbH, Konstanz, Germany.
[5]CNS Disease Research, Boehringer Ingelheim Pharma GmbH & Co. KG, Biberach an der Riss, Germany.
[6]Institute of Chemistry, University of Potsdam, Potsdam, Germany.
*These authors contributed equally to this work.

Innovation

The well-studied parkinsonian toxicant, 1-methyl-4-phenyl-tetrahydropyridine (MPTP), requires astrocytic metabolism to generate 1-methyl-4-phenyl-pyridinium (MPP^+). Subsequently, MPP^+ is transported into dopaminergic neurons by dopamine transporters (DATs) and it thereby accumulates and eventually kills these cells. Why MPP^+ spares the astrocytes in which it is supposedly generated and how MPP^+ leaves these cells have been a vexing enigma for decades. We found here that MPP^+ is generated extracellularly and that the release of its membrane-permeable precursor 1-methyl-4-phenyl-2,3-dihydropyridinium ($MPDP^+$)/1-methy-4-phenyl-1,2-dihydropyridine (1,2-MPDP) from astrocytes is transporter independent. Differences in O_2 and pH between the intra- and extracellular environment favor the stabilization of the labile MPTP intermediate, $MPDP^+$/1,2-MPDP, within astrocytes and promote its nonenzymatic conversion in the extracellular space.

MPTP is a lipophilic and noncytotoxic prodrug that crosses the blood–brain barrier and is then converted into the active toxicant MPP^+ (23, 32, 54). Once MPP^+ reaches a critical concentration in the cerebrospinal fluid, it acts as a molecular ''Trojan Horse'' in DA neurons as a result of its selective uptake by the dopamine transporter (DAT) (26). Unlike DA, MPP^+ accumulates in mitochondria, where it acts as an inhibitor of complex I of the respiratory chain (38) and thereby kills its host cell (10). However, a vexing enigma pertaining to the neurotoxic mechanisms of MPTP remains unsolved. MPTP is converted to MPP^+ in astrocytes by the enzyme, monoamine oxidase-B (MAO-B), which is localized on the outer mitochondrial membrane of astrocytes (44). How MPP^+ exits astrocytes rather than accumulating in their mitochondria is unknown.

Due to its charge, the active toxicant MPP^+ cannot cross membranes. Recent reports have suggested that passive transporters, such as the family of organic cation transporters (OCTs) or the plasma membrane monoamine transporter, are necessary for MPP^+ efflux from astrocytes (9, 37). OCT3 was observed by Cui *et al.* to be preferentially expressed in glial cells in the vicinity of midbrain DA neurons that degenerated in response to MPTP treatment, and it was hypothesized that a preferential export of intracellular astrocytic MPP^+ *via* OCT3 might contribute to the loss of adjacent DA neurons (9). However, a recent study clearly demonstrated the global formation of MPP^+ in the whole brain only minutes after MPTP administration and a subsequent rapid clearance from most regions (28). This indicates that glial cells devoid of OCT3 expression must also contribute to MPTP conversion and MPP^+ release. Moreover, conventions in membrane biophysics suggest that passive transporters such as OCT3 would contribute to an uptake of MPP^+ from the cerebrospinal fluid into cells (49). A plasma membrane potential of −70 mV would drive a 15-fold increase in the accumulation of a positively charged molecule inside cells according to the Nernst equation. Hence, the presence of OCTs in glial cells would rather lead to a reduction of extracellular MPP^+ and its toxicity in neurons, as it was observed with monovalent paraquat (42).

MPTP can form several metabolites other than MPP^+ in the brain (52) and their biochemical and physical properties need to be taken into account to understand the possible mechanisms of MPP^+ transport across the membrane. The first metabolic step in MPP^+ formation is always an MAO-dependent two-electron oxidation yielding the unstable intermediate $MPDP^+$ (5). A nonenzymatic autoxidation of $MPDP^+$ has been suggested as the most likely second step of MPP^+ formation (30). In addition, a disproportionation reaction yielding one molecule of MPTP and MPP^+ from two molecules of $MPDP^+$ has been described (4, 39). However, this reaction takes place only at concentrations of $MPDP^+$ (millimolar range) unlikely to occur in biological systems. The complex chemistry of $MPDP^+$ involves further spontaneous reactions; as an α,β-unsaturated iminium ion, $MPDP^+$ can exist in tautomeric forms, and/or in its conjugate base form, 1,2-MPDP (4, 5). The latter noncharged metabolite is capable of crossing biological membranes.

In the present work, we report two main findings: (1) the MAO-catalyzed MPTP intermediate metabolite, $MPDP^+$/1.2-MPDP, undergoes transporter-independent export from the cell and (2) $MPDP^+$/1.2-MPDP is responsible for nonenzymatic MPP^+ formation in the extracellular space. These mechanisms explain why MPTP-converting glial cells are spared from MPP^+ toxicity and how extracellular MPP^+ is generated, which is a necessary prerequisite for the accumulation of MPP^+ in catecholaminergic cells.

Results

Extracellular MPP^+ generation by MPTP-converting astrocytes predominates

We studied the conversion of MPTP to MPP^+ by astrocytes in the mouse astrocytic cell line, immortalized mouse astrocyte (IMA) 2.1, which displays MPTP metabolism properties comparable with primary astrocytes [Fig. 1A, B (45)]. We observed an accumulation of the biologically active toxicant MPP^+ in the IMA culture medium, but not within the cells (Fig. 1C, D). Addition of the OCT3 inhibitor, D22, to the culture medium had no influence on MPP^+ release or uptake (data not shown), suggesting that the previously suggested OCT3 transport mechanism (9) was not obligatory for extracellular MPTP/MPP^+ accumulation. However, the MPTP-converting enzyme, MAO-B, is located exclusively within the astrocytic cell body, and MPP^+, as a charged molecule, cannot penetrate biological membranes. This raises the following question: How can MPP^+ be efficiently generated extracellularly in the absence of a system for its transport from the cell (Fig. 1C)?

To resolve this issue, we generated IMA subclones that stably express OCT3 (a passive transporter of MPP^+), DAT (accumulates MPP^+ against a concentration gradient), or both DAT and OCT3; these cells lines are referred to as OCT3-IMA, DAT-IMA, and OCT3/DAT-IMA, respectively. Expression levels of OCT3 in the OCT3-IMA and OCT3/DAT-IMA lines were identical (Supplementary Fig. S1A; Supplementary Data are available online at www.liebertpub.com/ars), and the transport capacity and pharmacological features were comparable with those of the human kidney carcinoma cell line, Caki-1, which endogenously expresses OCT3 (22). We next assessed MPP^+ transport in these cell lines. In DAT-IMAs, uptake of MPP^+ was prevented by the

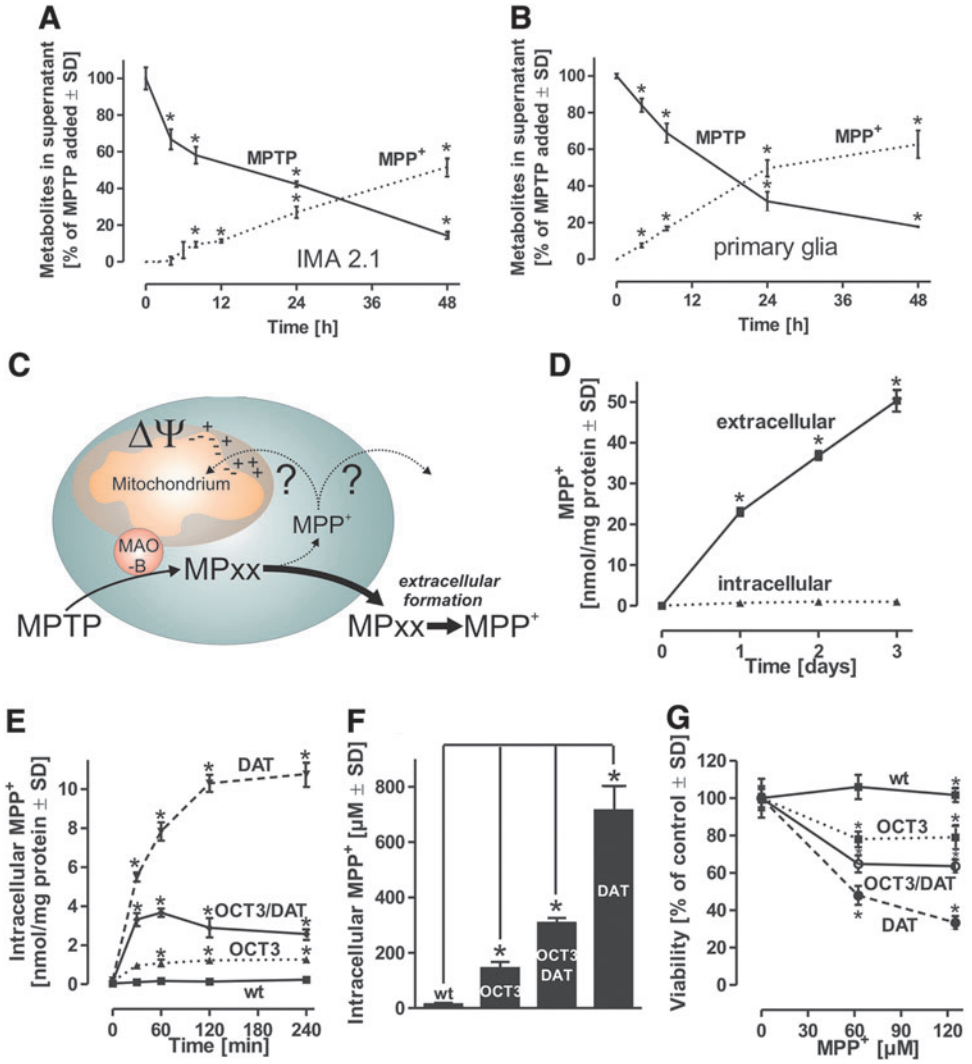

FIG. 1. Formation and release of MPP+ by astrocytes. The mouse astrocyte cell line, IMA 2.1 **(A)**, and primary mouse glial cells **(B)** were incubated with MPTP (30 μM) for the indicated time intervals. MPTP and MPP+ were measured in the supernatant by high performance liquid chromatography (HPLC) analysis. **(C)** A schematic overview of MPTP conversion by astrocytes. In the first step, MPTP is oxidized by mitochondrial MAO-B. In the second step, the intermediate undergoes a nonenzymatic autoxidation to form MPP+. Intracellular formation of MPP+ would imply either an accumulation within mitochondria driven by their membrane potential ($\Delta\Psi$) or a transporter-mediated passage across the membrane. The primary export mechanism for MPTP metabolites we propose herein assumes the formation of a membrane-permeable intermediate that diffuses across the plasma membrane and ultimately forms MPP+ in the extracellular space. **(D)** IMAs were exposed to MPTP (20 μM) for the time intervals indicated, and intracellular and extracellular (supernatant) MPP+ levels were analyzed. **(E)** IMA wild-type cells (wt) or transgenic cells stably expressing the OCT3, the DAT, or a combination of both were exposed to MPP+ (20 μM) for the time periods indicated, and intracellular MPP+ was measured. **(F)** IMA clones were exposed to MPP+ (20 μM) for 2 h to allow for saturation of uptake. Intracellular MPP+ concentrations were calculated from measured MPP+ amounts in cell homogenates and cell volumes that were in the range of 2.5 pl/cell. **(G)** IMA transgenic cells expressing OCT3, DAT, or a combination of both were exposed to varying MPP+ concentrations for 24 h, viability was then assessed by the resazurin reduction assay. All data are mean ± SD ($n = 3$) *$p < 0.05$. DAT, dopamine transporter; IMA, immortalized mouse astrocytes; MAO-B, monoamine oxidase B; MPP+, 1-methyl-4-phenyl-pyridinium; MPTP, 1-methyl-4-phenyl-tetrahydropyridine; OCT3, organic cation transporter-3; SD, standard deviation. To see this illustration in color, the reader is referred to the web version of this article at www.liebertpub.com/ars

DAT blocker, GBR12909, while in OCT3-IMAs, MPP+ uptake was prevented by the OCT3 blocker, D22 (Supplementary Fig. S1A–D).

We next assessed the response of wild-type and the transporter-expressing cell lines to MPP+ treatment. All cells were exposed to a fixed concentration (20 μM) of extracellular MPP+ (Fig. 1E). The toxicant did not enter wild-type IMAs, which was as expected given the absence of functional carriers in the plasma membrane in these cells and the inability of MPP+ to cross lipid bilayers. Strong intracellular accumulation was, however, observed in DAT-IMAs. Ectopic OCT-3 expression in OCT3-IMAs and OCT3/DAT-IMAs enabled influx of MPP+ into cells. In OCT-3/DAT-IMAs, MPP+ efflux from cells that had accumulated very high

concentrations of MPP^+ due to DAT activity was observed (Fig. 1E). Steady-state levels were reached within 2 h. At this time point, the absolute amount of accumulated MPP^+ was measured and the cellular volume of IMAs was determined (2.5 pl/cell) so that average intracellular MPP^+ concentrations could be calculated (Fig. 1F). The transporter-expressing cells reached levels of around 180–680 μM, which are highly similar to tissue concentrations found in mice exposed to MPTP (19). Within 24 h, these concentrations were sufficient to diminish the cellular capacity to reduce resazurin or to produce ATP (Supplementary Fig. S2). By contrast, IMAs neither accumulated MPP^+ nor displayed impaired viability in response to up to a 120 μM concentration of extracellular MPP^+. Indeed, the degree of MPP^+-induced reductions in viability across the four cell lines correlated with their respective capacity to accumulate MPP^+ (Fig. 1G). These data support the notion that astrocytes are not resistant to MPP^+ toxicity as reduced viability was observed as soon as MPP^+ accumulated within the transporter-expressing cells. Our findings also confirm that MPP^+ cannot cross the membranes of IMAs unless they ectopically express MPP^+ transporters. This led us to posit that MPP^+ crossed the IMA membrane through an OCT-3-independent mechanism during the course of MPTP metabolism.

$MPDP^+$ is a membrane-crossing intermediate generated from MPTP by MAO-B

Since the pioneering work of Castagnoli et al., it has been known that MAO-B converts MPTP to intermediates such as $MPDP^+$ and that further oxidation to MPP^+ proceeds nonenzymatically (4, 30, 39). Some of these initial publications speculated that these intermediates might play a role in transport processes, but further investigation of their biological formation and properties over the last 30 years has been highly limited. We thus focused here on the transport of $MPDP^+$ as a potential missing link that might explain extracellular MPP^+ formation. Analysis of the products formed in the conversion of MPTP by purified MAO-B enzyme confirmed that $MPDP^+$ is a major intermediate in the generation of MPP^+ (Fig. 2A). Similar observations were made in the analysis of wild-type IMA and OCT3-IMA cultures treated with MPTP as $MPDP^+$ was detected in the supernatant before MPP^+. We further found that $MPDP^+$ export was not dependent on OCT3 (Fig. 2B). To determine if $MPDP^+$ formation in this *in vitro* model also occurs *in vivo*, mice were injected with MPTP and the striatum and cerebellum were collected from injected mice at different time intervals. These experiments revealed a rapid (30 min) rise of $MPDP^+$ in both brain areas that preceded the formation of MPP^+. MPP^+ remained elevated in the striatum, but not in the cerebellum (Fig. 2C). C-5 carbons of tetrahydropyridine structures such as $MPDP^+$ are acidic (*i.e.,* they possess an α,β-unsaturated iminium ion structure). However, their conjugate free base form, 1,2-MPDP, was also observed (4, 30, 39) (Fig. 2D) and this molecule is expected to be able to freely diffuse across biological membranes. To more carefully examine the formation of intermediates that are generated in the MAO-dependent conversion of MPTP to MPP^+, we conducted time-resolved ^{1}H-NMR analysis (Supplementary Fig. S3). These data confirmed a significant time lag between the enzymatic formation of $MPDP^+$ and its subsequent autoxidation to MPP^+. Based on these findings, we hypothesized that the acid–base pair, $MPDP^+$/1.2-MPDP, serves as a membrane-permeable intermediate in MPP^+ production that is exported from astrocytes and would thereby explain the presence of extracellular of MPP^+.

Free bidirectional flux of $MPDP^+$/1.2-MPDP across biological membranes

To test the hypothesis that $MPDP^+$/1.2-MPDP possesses transporter-independent membrane permeability, IMAs were treated with 50 μM fresh $MPDP^+$ or decomposed $MPDP^+$ (stored in an open tube at room temperature before use). Both the resazurin reduction assay and measurements of intracellular ATP (Fig. 2E) indicated that only fresh $MPDP^+$ led to cell damage. For an appropriate interpretation of the data, it is important to note that the extracellular volume in these experimental setups is substantially greater than the intracellular volume. Treatment of the cells with MPTP hence results in a constant and steep concentration gradient of freshly generated $MPDP^+$ that supports its efflux into the extracellular space. In contrast, extracellular addition of $MPDP^+$ generates conditions in which the intracellular volume is rapidly saturated (*i.e.,* intracellular volume <<< extracellular volume).

To confirm a direct influence of intracellular MPP^+ on mitochondria, metabolic flux measurements were obtained as a more sensitive readout. MPP^+ specifically inhibits complex I of the electron transport chain. As a result, nicotinamide adenine dinucleotide (reduced) (NADH) cannot be oxidized *via* complex I and accumulates in the cell. An increase in the NADH (reduced)/NAD^+ (oxidized) ratio results in an inhibition of NAD^+-dependent reactions of the TCA cycle, such as pyruvate dehydrogenase activity. In the case of complex I inhibition, glucose carbon contribution to the TCA cycle strongly decreases, while pyruvate reduction to lactate increases. By increasing the rate of glycolysis, the cell compensates for the lack of ATP, similar to the Warburg effect. To assess metabolic flux, we labeled cells with the tracer [U-$^{13}C_6$] glucose, which can be used to monitor relative pyruvate oxidation that results from the NAD^+-dependent pyruvate dehydrogenase reaction decarboxylating pyruvate in the mitochondrion during the production of acetyl-CoA (Fig. 2F). The activities of pyruvate dehydrogenase and of ATP-dependent pyruvate carboxylase were both inhibited by $MPDP^+$, but not by MPTP or MPP^+ (Fig. 2F, Supplementary Fig. S4).

To directly compare MPP^+ and $MPDP^+$ uptake, intracellular MPP^+ levels in IMAs exposed to either MPP^+ or $MPDP^+$ were investigated. To exclude any potential involvement of cellular transporter systems, all experiments were conducted in parallel with artificial lipid vesicles (Fig. 3A). As a third model system, purified human erythrocytes were used as they possess no MPP^+ transporter activity, but do allow the conversion of $MPDP^+$ to MPP^+ due to the presence of iron-containing hemoglobin. In all three model systems, extracellular concentrations of MPP^+ as high as 200 μM did not result in significant accumulation of intracellular MPP^+, while the addition of $MPDP^+$ immediately led to the formation of intracellular/intravesicular MPP^+. Uptake of $MPDP^+$ and MPP^+ into erythrocytes was then tested *in vivo* by intravenous injection of these compounds into mice and collection of blood after 3 min. Similar to the *ex vivo* treatment of erythrocytes, the addition of $MPDP^+$ resulted in the

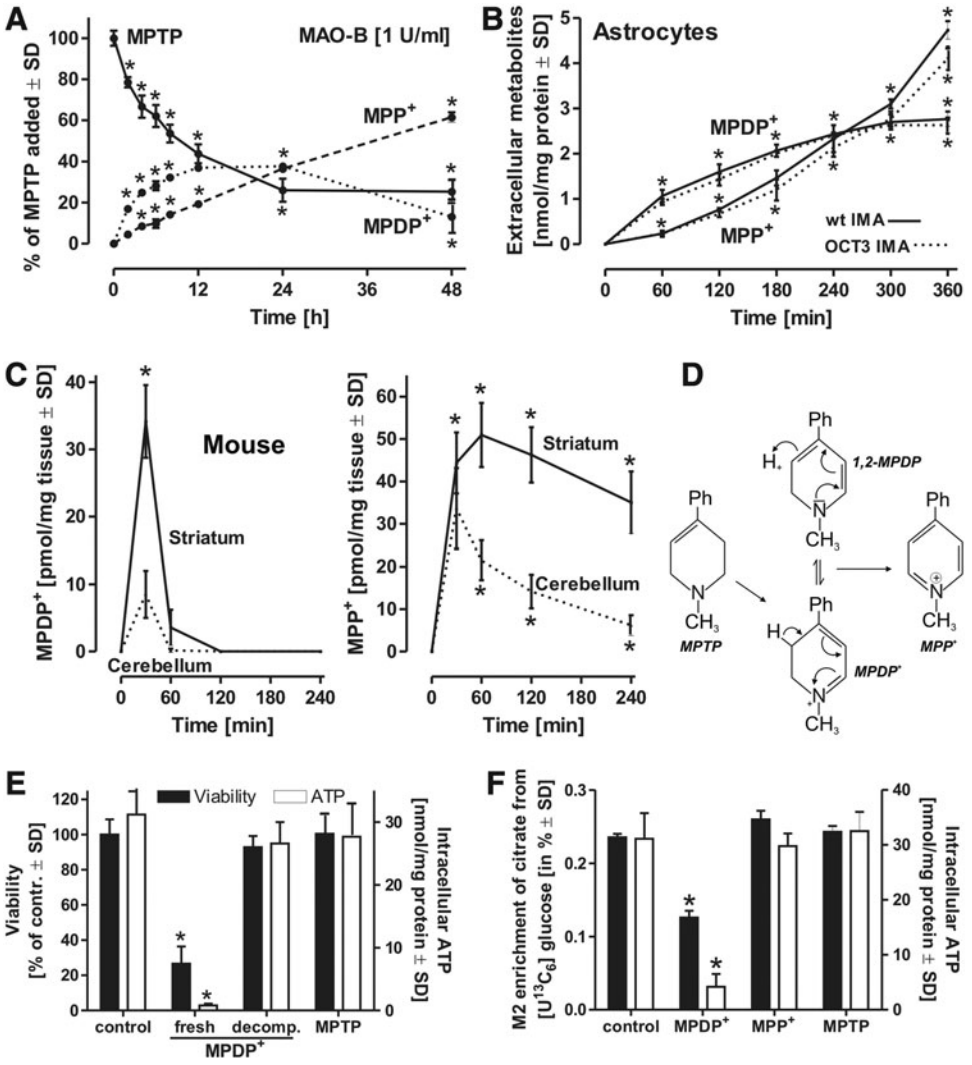

FIG. 2. MPDP$^+$ generation precedes the formation of MPP$^+$ *in vitro* and *in vivo*. **(A)** Purified MAO-B enzyme (1 U/ml) was incubated with 30 μM MPTP for the time intervals indicated. In addition to MPP$^+$, an intermediate was detected that was identified as MPDP$^+$. **(B)** Wild-type (wt) IMAs or OCT3-expressing IMAs were treated with MPTP (30 μM) for various incubation periods, and MPP$^+$ and MPDP$^+$ levels in the extracellular medium were assessed. **(C)** Mice received an intraperitoneal injection of MPTP (30 mg/kg) at $t = 0$ min. After the time intervals indicated, samples from the striatum and the cerebellum were collected and analyzed by HPLC. **(D)** Structures of MPTP and its derivatives are shown. MPDP$^+$ originates from the MAO-B-catalyzed two-electron oxidation of MPTP. Under physiological conditions, MPDP$^+$ can also exist in its uncharged and membrane-permeable base form, 1,2-MPDP. This intermediate is converted by nonenzymatic autoxidation into MPP$^+$. **(E)** IMAs were incubated with 50 μM of MPTP, MPDP$^+$, or decomposed MPDP$^+$ for 18 h. Cell viability was detected by the resazurin reduction assay and by analysis of intracellular ATP. **(F)** For an analysis of intracellular fluxes of central carbon metabolism, IMAs were incubated with [U-$^{13}C_6$] glucose and treated with MPTP or MPDP$^+$ (50 μM) for 18 h. All data are mean ± SD ($n = 3$) *$p < 0.05$. 1,2-MPDP, 1-methy-4-phenyl-1,2-dihydropyridine; MPDP$^+$, 1-methyl-4-phenyl-2,3-dihydropyridinium.

intracellular accumulation of MPP$^+$, providing further evidence of transporter-independent membrane passage of MPDP$^+$ (Supplementary Fig. S5).

To further test the kinetics of cell loading and unloading of MPDP$^+$, IMAs were exposed to MPDP$^+$ (50 μM) for a 30-min loading phase. Analysis of the cellular compartment showed a rapid increase of MPDP$^+$, followed by a rise in MPP$^+$ concentrations. MPP$^+$ was apparently generated within these cells as extracellular MPP$^+$ cannot cross the cell membrane (Fig. 3B, *Left*). After the loading phase, cells were washed, new medium was added, and metabolite levels were detected over time in both the intracellular (Fig. 3B, *Middle*) and extracellular compartments (Fig. 3B, *Right*). Accumulated MPDP$^+$ vanished rapidly from the cells into the extracellular media, whereas intracellular MPP$^+$ was not able to exit the cells (Fig. 3B, *Middle and Right*). Considering these data together, we concluded that extracellular MPP$^+$ originated from the autoxidation of extracellular MPDP$^+$. In addition, these findings indicate that the MPDP$^+$ concentration gradient is the predominant driving force underlying its transport across membranes, which explains the apparent export of MPP$^+$. These observations indicate that MPDP$^+$/1.2-MPDP is membrane

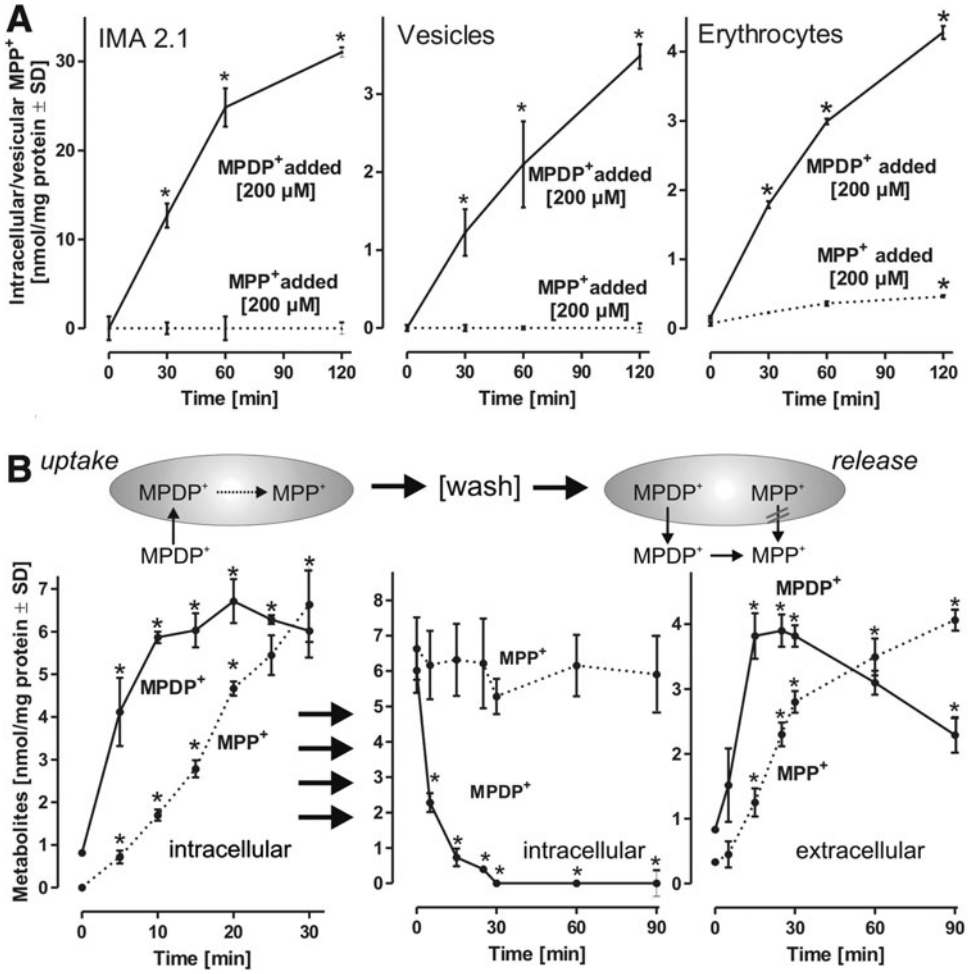

FIG. 3. The intermediate MPDP$^+$ crosses biological membranes. (A) Uptake velocities of MPP$^+$ and MPDP$^+$ were investigated by detecting intracellular MPP$^+$ in IMAs incubated with 200 μM of the compound for various time intervals. To exclude the involvement of cellular transporters or mitochondrial transmembrane potential, the same experimental setup was conducted with artificial vesicles comprising 50 mol% DOPC and 50 mol% DOPE. Human erythrocytes were used as an alternative cellular model with high endogenous iron content (hemoglobin), which facilitates the intracellular conversion of MPDP$^+$. **(B)** Bidirectional transport of MPDP$^+$ across biological membranes was studied in IMAs loaded with 50 μM MPDP$^+$ over the course of 30 min (*left*). Cells were then washed thrice, new medium was added, and the release of intracellular MPDP$^+$ and MPP$^+$ (*middle*) into the medium (*right*) was detected. All data are mean ± SD ($n = 3$) *$p < 0.05$. DOPC, 1,2-dioleoyl-*sn*-glycero-3-phosphatidylcholine; DOPE, 1,2-dioleoyl-*sn*-glycero-3-phosphoethanolamine.

permeable and suggest that MPP$^+$ will remain in a given biological compartment, unless transporters are present.

The role of extracellular MPDP$^+$ autoxidation in dopamine neuron toxicity

Our data heretofore have suggested that upon MPTP intoxication, MPDP$^+$/1.2-MPDP would have the potential to freely diffuse across the membranes of several cells and eventually convert to MPP$^+$ in any cell type adjacent to MAO-containing glial cells. However, MPP$^+$ accumulation is largely limited to catecholaminergic neurons that take up the molecule *via* their catecholamine transporter (*e.g.,* DAT). To compare the respective contribution of DAT-mediated MPP$^+$ accumulation and passive MPDP$^+$/1.2-MPDP-dependent influx (Fig. 4A), human dopaminergic neuronal cells, lund human mesencephalic neuron (LUHMES), which can accumulate extracellular MPP$^+$ *via* DAT (46, 47, 48), were treated with MPP$^+$ or MPDP$^+$ (20 μM) in the presence or absence of the DAT blocker, GBR12909 (GBR). This compound blocks the uptake of MPP$^+$ *via* DAT inhibition, but not MPDP$^+$/1.2-MPDP as it is not a DAT substrate. Metabolic flux was measured with labeled [U-$^{13}C_6$] glucose, which provides a readout of the inhibition of oxidative phosphorylation. Both MPP$^+$ and fresh MPDP$^+$ led to mitochondrial inhibition, and GBR blocked toxicity in both cases (Fig. 4B). These observations were confirmed by cellular staining with an anti-β-III-tubulin antibody, which demonstrated that pronounced neurite degeneration was triggered by both MPP$^+$ and fresh MPDP$^+$, and these effects were completely prevented by GBR (Fig. 4C). Taken together, these data suggest that at the moderate MPDP$^+$/1.2-MPDP concentrations (low micromolar range) that exist *in vivo*, intracellular autoxidation of MPDP$^+$ would not be sufficient to generate damaging intracellular MPP$^+$ concentrations.

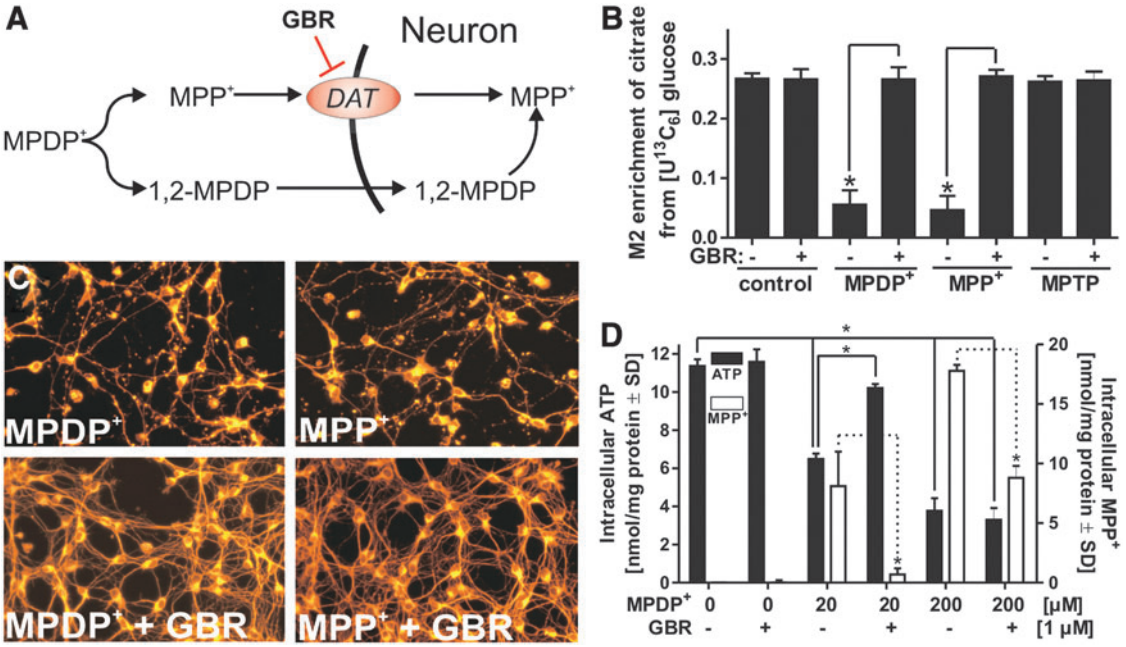

FIG. 4. Transporter-independent uptake of MPDP$^+$ into dopaminergic neurons. (A) Neuronal LUHMES cells endogenously expressing the DAT allow either a transporter-independent uptake of the MPDP$^+$/1,2-MPDP intermediate, followed by intracellular autoxidation into MPP$^+$, or a DAT-dependent uptake of MPP$^+$ originating from the extracellular autoxidation of MPDP$^+$/1.2-MPDP. **(B)** As a sensitive readout for mitochondrial activity, glucose oxidation was monitored in LUHMES cells treated with MPP$^+$ or MPDP$^+$ (20 μM) by the addition of [U-$^{13}C_6$] glucose in the presence or absence of the DAT blocker, GBR (1 μM), for 18 h. **(C)** The morphology of LUHMES cells treated with MPP$^+$ or MPDP$^+$ (20 μM) in the presence or absence of GBR (1 μM) for 24 h was visualized by staining with an anti-β-III-tubulin antibody. **(D)** To determine the respective contribution of DAT-dependent and independent uptake, LUHMES cells were incubated in low (20 μM) or high (200 μM) MPDP$^+$ concentrations. Intracellular levels of ATP and MPP$^+$ were detected after 24 h. All data are mean ± SD ($n = 3$) *$p < 0.05$. LUHMES, lund human mesencephalic neuron. To see this illustration in color, the reader is referred to the web version of this article at www.liebertpub.com/ars

To explore whether toxic MPP$^+$ can be formed within neurons from freely diffusing and autoxidizing MPDP$^+$, LUHMES cells were exposed to high (200 μM) or low (20 μM) MPDP$^+$ concentrations in the presence or absence of the DAT blocker, GBR. High extracellular MPDP$^+$ levels led to a DAT-independent accumulation of intracellular MPP$^+$ doses sufficient to inhibit mitochondria, whereas low concentrations did not (Fig. 4D). Thus, toxicity evoked by free diffusion of freshly generated MPDP$^+$ in cells adjacent to astrocytes may play only a marginal role. To test this assumption, a coculture model containing IMAs (astrocytes) and LUHMES (neurons) was exposed to MPTP. This led to neurotoxicity *via* glial-dependent generation of MPP$^+$. The addition of GBR completely inhibited neurotoxicity in this coculture system. These data confirm that the passive diffusion of freshly generated MPDP$^+$/1.2-MPDP itself from glia immediately adjacent to LUHMES cells was not able to evoke significant toxicity (Supplementary Fig. S6).

Identification of physiological factors that promote the autoxidation of MPDP$^+$ in the extracellular space

The findings described thus far indicate that MPP$^+$ needs to be formed extracellularly to become a substrate for DAT and thus induce neurotoxicity. We next explored how a preferential extracellular generation of MPP$^+$ might proceed in structures such as the brain with a high ratio between the intra- and the extracellular volume. As oxygen levels are likely to play a role in MPDP$^+$ autoxidation, we studied this environmental factor. High-resolution measurements of oxygen concentrations in cells have provided evidence for steep oxygen concentration gradients between the cytosol and mitochondria (27, 36). This may result in average intracellular oxygen concentrations that are significantly lower than the interstitial levels in tissue or cell culture media (17, 51). We found that the speed of MPP$^+$ formation strongly depended on oxygen levels and that MPDP$^+$ is highly stable under low oxygen conditions such as those that are typically found near the respiring mitochondria (27, 36, 51) of astrocytes (Fig. 5A, B). Lower intracellular oxygen levels would hence stabilize intracellular MPDP$^+$, while at the higher extracellular oxygen tension, the nonenzymatic conversion into MPP$^+$ would be favored.

We posited that another important factor in determining the rate of MPDP$^+$ autoxidation might be the local pH. The cytosolic pH of most cells in the body is typically lower than in extracellular fluids and the blood. Local acidification is largely driven by respiratory chain proton pump activity, particularly around mitochondria. We observed an accelerated autoxidation of MPDP$^+$/1.2-MPDP under more alkaline conditions (Fig. 5C, D), while more acidic conditions (*e.g.,* close to mitochondria) stabilized MPDP$^+$. The combination of a more acidic pH and lower oxygen tensions (*e.g.,* the conditions typically encountered inside cells) strongly prevented MPDP$^+$ autoxidation (Fig. 5E, F).

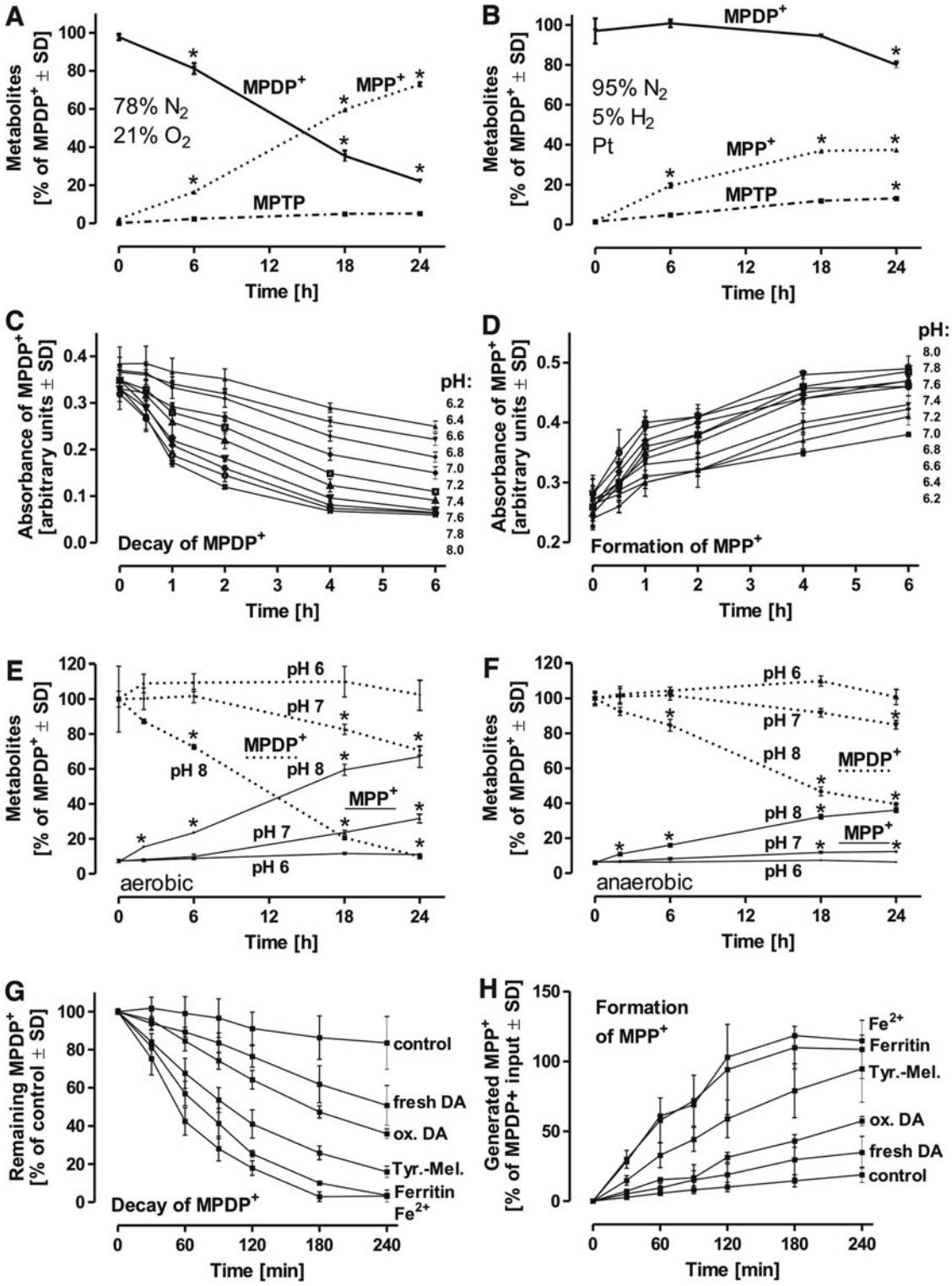

FIG. 5. Modulation of the nonenzymatic conversion of $MPDP^+$ into MPP^+. **(A)** $MPDP^+$ (100 μM) was kept under atmospheric conditions in DMEM medium at 37°C or under oxygen-free conditions **(B)** for the time intervals indicated. MPP^+, $MPDP^+$, and MPTP were detected by HPLC. **(C, D)** $MPDP^+$ (100 μM) was maintained in potassium phosphate buffer with varying pH, as indicated in each time interval. Autoxidation of $MPDP^+$ into MPP^+ was monitored photospectrometrically. **(E, F)** $MPDP^+$ (100 μM) was kept under atmospheric **(E)** or oxygen-free conditions **(F)** in potassium phosphate buffer of different pH at 37°C for the indicated incubation intervals. **(G, H)** To identify the influence of metabolites of the dopamine pathway and physiologically relevant iron-containing molecules, $MPDP^+$ (100 μM) was treated with the indicated compounds (100 μM each) under aerobic conditions with a pH of 7.4. All data are mean ± SD ($n = 8$) $^*p < 0.05$.

Based on these findings, we hypothesized that in addition to DAT activity, the conditions in brain regions enriched in dopaminergic neurons might promote greater autoxidation than in other areas. The nigrostriatal system of the basal ganglia has a particularly high iron content and also contains various autoxidation products of dopamine (12, 35). All of these compounds promote the formation of radicals, which are required for autoxidation of $MPDP^+$. While free radicals have very short half-lives inside cells due to several efficient free radical buffering mechanisms (*e.g.,* glutathione system, iron buffering), they can persist for longer times extracellularly. Taking this into consideration, several candidates were tested for their influence on $MPDP^+$ autoxidation. A striking acceleration of MPP^+ genesis from $MPDP^+$ was observed in response to the treatment with autoxidized dopamine, melanin, iron-containing ferritin, or with free ferrous iron (Fig. 5G, H). Addition of the iron chelator, deferoxamine, prevented the iron-mediated acceleration of $MPDP^+$ autoxidation (Supplementary Fig. S7). This is in accordance with reports indicating a protective role of iron chelators in MPTP PD models (11, 29), although these reports did not demonstrate whether the conversion of MPTP was affected by treatment with iron chelators or other oxidative stress-related events. Enhanced autoxidation in the extracellular milieu would not only explain preferential MPP^+ generation outside cells but also ensures there is a constant, steep concentration gradient between cytosolic $MPDP^+$ and extracellular $MPDP^+$, which is the main driving force for its transporter-independent efflux (Fig. 6).

Discussion

Among the known human neurotoxicants, MPTP is exceptional, in that it triggers relatively selective death of nigrostriatal DA neurons upon systemic administration (3, 25, 31). A necessary prerequisite for the selective DAT-dependent uptake of the active toxin MPP^+ is the presence of MPP^+ in the extracellular space, as was elegantly confirmed by several microdialysis studies (9, 21, 33). The mechanism by which MPP^+, a membrane-impermeable molecule generated intracellularly by the enzymatic conversion of MPTP, reaches the extracellular space has been elusive. The present work aimed at addressing this question and was inspired by the observation of efficient extracellular MPP^+ generation in MPTP-converting astrocytes in the absence of significant intracellular MPP^+ accumulation and toxicity.

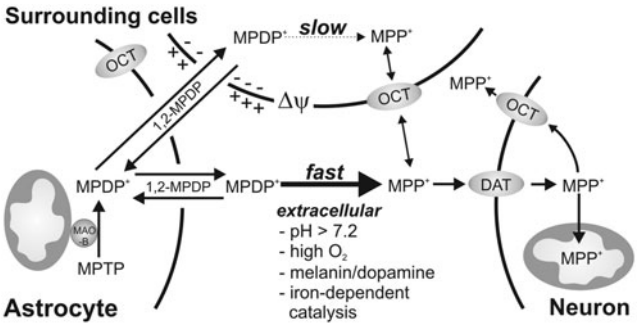

FIG. 6. $MPDP^+$/1,2-MPDP is the main exported form of MPTP metabolites. MAO-B-dependent conversion of MPTP in astrocytes yields $MPDP^+$ that partially exists in its conjugate base form, 1,2-MPDP, and is able to freely diffuse across biological membranes. Conditions with an alkaline pH, elevated O_2 tension, iron-containing proteins, or neuromelanin promote accelerated autoxidation of $MPDP^+$ in the extracellular space. Due to its charge, stable MPP^+ requires transporters such as the DAT or the OCT for cellular uptake.

We first determined that astrocytes (IMAs) were not immune to MPP^+ as these cells died when cytosolic accumulation of extracellular MPP^+ was enabled by the ectopic expression of the MPP^+ transporters, DAT and/or OCT3. Although it can be concluded from these results that astrocytes are not *per se* resistant to MPP^+, they do have the capacity to accelerate glycolytic turnover and hence are able to at least partially compensate for inhibited mitochondrial ATP synthesis caused by MPP^+. This conclusion is corroborated by several experiments in the literature showing that any cell tested thus far, for example, HEK293, hepatocytes, COS, or HeLa cells, is killed by MPP^+ if the toxicant is allowed to enter the cytosol.

Moreover, the findings of the present study provide a rationale for why cells that metabolize MPTP with endogenous MAO, such as astrocytes, platelets, and hepatocytes, are not necessarily killed by the final reaction product, MPP^+. We found that the intermediate $MPDP^+$ (or its neutral base 1.2-MPDP) exits cells along a concentration gradient *via* membrane diffusion. MPP^+ is mainly formed extracellularly and, in most cases, it would be diluted and carried away by body fluids or taken up by passive transporters in neighboring cells. In most cells, MPP^+ accumulation would therefore be transient and minimal as $MPDP^+$/1.2-MPDP would exit the cell as soon as the extracellular concentration drops. Only cells that accumulate MPP^+ through an active intracellular transport mechanism, for example, DA neurons in the central nervous system, would therefore be able to retain the toxicant for a sufficient period of time and at high enough concentrations to cause damage (Fig. 6). While accumulation of MPP^+ in cells is a necessary condition for the toxicity of this molecule, the degree of susceptibility of particular cell types to intracellular MPP^+ may vary due to the presence or absence of resistance mechanisms, for example, by sequestration as in adrenomedullary cells (43) or other more poorly understood cellular factors (7, 46). Alternatively, certain cells may possess factors that promote MPP^+ formation and toxicity; for instance, cytochrome P-450 2D6 was recently suggested to directly contribute to the conversion of MPTP in neuronal cells (1). By contrast, in LUHMES cells, MPTP treatment resulted in neither the formation of MPP^+ nor cellular degeneration (not shown).

The concentration of MPP^+ required to cause toxicity in different cell types may therefore vary. Studies of isolated mitochondria and submitochondrial particles have shown that MPP^+ concentrations of about 5–20 mM need to be reached in the mitochondrial matrix for inhibition of complex I (40, 41), which would in turn require cytosolic levels in the high micromolar range (>100 μM). This is corroborated by our measurements showing mitochondrial effects and toxicity within a period of 24–48 h in IMAs expressing OCT3 or DAT if intracellular MPP^+ concentrations were larger than 100 μM (Fig. 1F). By contrast, our measurements of wild-type IMAs showed that concentrations were $\sim 10\ \mu$M ($\approx$ 1 nmol/mg protein), which is in close accordance with the

data of Di Monte *et al.* obtained from primary mouse astrocyte cultures (1 nmol/mg after a 48-h exposure to 250 μM MPTP) (15, 16, 55).

In this study, we have demonstrated that $MPDP^+$ is the pivotal MPTP metabolite responsible for the extracellular genesis of MPP^+, which minimizes its toxicity to most cell types. $MPDP^+$ was described and synthesized by Castagnoli et al. in the 1980s (4, 5). Their pioneering discovery of this metabolite and the seminal work of Di Monte *et al.* (13–16, 55) were quickly incorporated into all major toxicology textbooks, but experimental study of this compound has been virtually nonexistent for the past 25 years, despite its wide use in PD research during this time. In this study, we have advanced this early work by providing direct evidence by NMR and MS of $MPDP^+$ formation during MPTP to MPP^+ conversion by MAO-B. It was originally postulated that the disproportionation of two molecules of $MPDP^+$ into MPP^+ and MPTP would be the dominating mechanism of MPP^+ formation; however, our previous studies on the autoxidation of resynthesized $MPDP^+$ suggest that direct oxidation of $MPDP^+$ into MPP^+ dominates (4, 5). Although the mechanism of $MPDP^+$ autoxidation has not yet been fully elucidated, kinetic and thermodynamic principles observed in structurally related compounds allow us to postulate that the reaction sequence is as follows: in the initial step, a stabilized allyl radical is formed by the abstraction of a proton at C5 as a result of the interaction of $MPDP^+$ with molecular oxygen (O_2), transition metals, or free radical species (*e.g.,* dopamine autoxidation products) (Supplementary Fig. S8); in a second reaction, the allyl radical interacts with a second free radical species or O_2; when there is an interaction with O_2, C-5 would carry a peroxide group, which would render the carbon 6 acidic and hence trigger the release of a proton from C-6 (peroxometabolite); energetically, the elimination of the C-5 hydroperoxide substituent from the base form would strongly favor aromatization to the stable toxin MPP^+ (Supplementary Fig. S8); and the final step of proton abstraction from the peroxometabolite is favored under alkaline conditions. This sequence of events is strongly supported by our experimental observations indicating accelerated $MPDP^+$ autoxidation in the presence of high oxygen levels and transition metals and a relative stabilization under slightly acidic conditions (Fig. 5). Importantly, autoxidation can efficiently proceed under conditions of relatively low $MPDP^+$ concentrations in contrast to disproportionation reactions.

We have identified several factors that increase MPP^+ formation in the extracellular space, most notably higher oxygen tension and pH. Indeed, the low oxygen levels within cells compared with the extracellular space may be reduced even further in astrocytes by MAO-B metabolism of MPTP, which is an oxygen-consuming reaction (6). Thus, low oxygen tensions and lowered pH around respiring astrocytes would prevent MPP^+ formation within cells, while this process would proceed faster in the extracellular space. Moreover, our data show that MPTP conversion proceeds more than 10 times faster in the presence of biological oxidation enhancers, such as melanin, oxidized dopamine, or ferrous iron. Some of these factors have particularly high levels not only in the nigrostriatal system, in which DA neurodegeneration prevails, but also in hemoglobin-carrying erythrocytes (Fig. 3A and Supplementary Fig. S5) (50, 53, 56). These factors are neutralized and scavenged to a large extent inside cells due to powerful redox buffers, lysosomal removal, or iron binding by ferritin, while they may exert their full activity in the extracellular space. Apart from oxygen tension or pH, other factors might indeed influence the autoxidation of $MPDP^+$. Our observation of accelerated $MPDP^+$ autoxidation induced by ferrous iron and its inhibition by the iron chelator, deferoxamine (Supplementary Fig. S7), provides insight into the molecular mechanisms that might underlie previous observations of protection against MPTP toxicity *in vivo* by iron chelator administration to model animals (11, 29). However, we tested ascorbic acid in a cell-free model of $MPDP^+$ autoxidation as well as in IMAs that were exposed to MPTP. In both cases, the autoxidation of $MPDP^+$ and the formation of MPP^+ were not affected (Supplementary Fig. S7). These findings indicate that a more detailed analysis of the molecular mechanisms involved is required.

A recent study reported that there is selective expression of OCT3 in glial cells located in close spatial vicinity to nigrostriatal neurons that were primarily affected in MPTP-challenged brains. This suggested that preferential MPP^+ release from astrocytes *via* OCT3 would be a major contributing factor in the selective loss of DA neurons in the *substantia nigra* (9). However, we observed that $MPDP^+$ generation in the brains of MPTP-treated mice preceded the formation of MPP^+ not only in the substantia nigra but also in the cerebellum, which is a prerequisite for the transporter-independent efflux of $MPDP^+$ into the extracellular space (Fig. 2). A recent publication was in full accordance with our findings in demonstrating almost uniform MPP^+ generation in MPTP-exposed brains only minutes after MPTP administration. This was followed by rapid clearance from the brain, except in the basal ganglia, ventral mesencephalon, and olfactory bulb (28). Given the findings that MPP^+ is generated globally in the extracellular space and taken up by specific cell types due to selective transporter expression, the tissue distribution of MPP^+ may be determined by complex dynamics that owe to the differential expression of MPP^+ transporters across cell types and brain regions. For instance, MPP^+ would be partially sequestered into cells expressing OCTs (Fig. 6), as indicated by our experiments with OCT-3-expressing IMAs (Fig. 1). Indeed, such a mechanism has been reported *in vivo* for the MPP^+-related compound, paraquat, which resulted in the protection of DA neurons in brains of paraquat-treated mice by lowering extracellular concentrations of the toxin (42).

The basic principles identified in the present work are not only limited to the experimental toxin, MPTP, but could also apply to endogenously formed small molecules, such as quinolinic acid (34), isoquinolines, beta-carbolines (8), or dopamine autoxidation products (2), all of which are suspected to play key roles in neurological and psychiatric disorders.

Materials and Methods

Materials

MPP^+ (1-methyl-4-phenyl-pyridinium-iodide), purified MAO-B, GBR12909 (DAT blocker), dopamine, ferritin, and tyrosine–melanin were purchased from Sigma-Aldrich (St. Louis, MO).

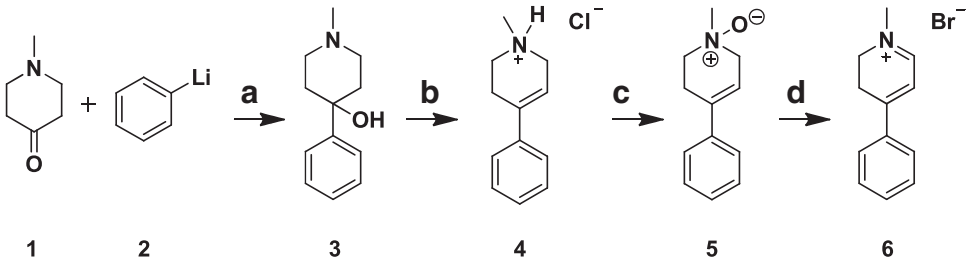

FIG. 7. Synthesis of MPTP-HCl (4) and MPDP+ bromide (6). **(a)** THF, –78°C → rt, overnight; (18) **(b)** aq HCl, reflux, 5 h, quantitative; (18) **(c)** (i) NaEtO, EtOH, 0°C (ii) aq H_2O_2, EtOH, 50°C, quantitative; (20) **(d)** DCM, TFAA, aq HBr, 0°C, 53%. (20). TFAA, trifluoroacetic anhydride; THF, tetrahydrofuran.

Synthesis of MPTP–HCl and MPDP+ bromide

All reagents are commercially available and were used without further purification. Solvents were dried over molecular sieves and used directly without further purification. All reactions were conducted under exclusion of air and moisture. ^{1}H- and ^{13}C-NMR spectra were recorded on an Avance III 400 MHz spectrometer from Bruker at room temperature. The time course of enzymatic MPTP conversion was followed on a Bruker AV III 600 MHz spectrometer equipped with a TCI cryoprobe. Spectra were processed with the software MestReNova 6.1.1 from MestRelab Research, and the ^{1}H and ^{13}C chemical shifts are reported relative to the residual solvent peak. High-resolution mass spectrometry (HRMS) was performed with micrOTOF-Q II ESI-Qq-TOF from Bruker Daltonics (Fig. 7).

Step a): 1-Methyl-4-phenyl-4-piperidinol **3** (18). A solution of 24.6 ml phenyllithium **2** (1.8 M in dibutyl ether) was added to a solution of 1-methyl-4-piperidone **1** (5 g, 44.19 mmol) in 20 ml of dry tetrahydrofuran at –78°C. The reaction was allowed to warm up to room temperature and was stirred overnight. The solvents were removed *in vacuo* to give crude **3** as a yellowish solid.

Step b): MPTP–HCl **4** (18). Refluxing of crude **3** in 50 ml 10% aq HCl for 5 h furnished compound **4**. The solvent was removed *in vacuo* and crude **4** was recrystallized from ethanol to give white crystalline **4** in a quantitative yield.

^{1}H-NMR (400 MHz, CD_3OD) δ 7.53–7.47 (m, 2H), 7.44–7.31 (m, 3H), 6.15 (ddd, J = 5.1, 3.4, 1.7 Hz, 1H), 4.08 (d, J = 15.3 Hz, 1H), 3.92–3.79 (m, 1H), 3.79–3.70 (m, 1H), 3.45–3.35 (m, 1H), 3.03 (s, 3H), 3.00–2.92 (m, 1H), 2.87 (d, J = 21.4 Hz, 1H).

^{1}H-NMR (600 MHz, D_2O) δ 7.55–7.52 (m, 2H), 7.46 (dd, J = 10.2, 4.8 Hz, 2H), 7.43–7.39 (m, 1H), 6.15–6.13 (m, 1H), 4.05 (d, J = 16.4 Hz, 1H), 3.82–3.78 (m, 1H), 3.74–3.69 (m, 1H), 3.43–3.34 (m, 1H), 3.00 (s, 3H), 2.96–2.90 (m, 1H), 2.86 (d, J = 19.0 Hz, 1H).

^{13}C-NMR (101 MHz, CD_3OD) δ 139.9, 136.8, 129.7, 129.4, 126.2, 116.6, 53.5, 52.0, 42.9, 25.8.

^{13}C-NMR (150 MHz, D_2O) δ 138.3, 134.6, 128.7, 128.4, 125.0, 115.5, 52.0, 50.6, 41.7, 23.8.

HRMS (ESI, positive ion mode): $[M+H]^+$; calculated: $C_{12}H_{15}N$: 174.1277 m/z; measured: 174.1288 m/z.

Step c): 1-Methyl-4-phenyl-1,2,3,6-tetrahydropyridine *N*-Oxide **5** (20).

(i) The solution of **4** (2.31 g, 11.01 mmol) in 60 ml ethanol was cooled to 0°C and 9.5 ml of a sodium ethoxide solution (1.17 M in ethanol, 11.12 mmol) was added. The mixture was filtered over celite and the filter cake was washed with 30 ml of ethanol.

(ii) Next, 2.6 ml of 30% aq H_2O_2 was added and *the mixture was stirred at 50°C. After 2 h, an additional portion of 2 ml* 30% aq H_2O_2 was added and it was stirred overnight. Afterward, the excess of H_2O_2 was quenched with 10% Pd/C. The resulting mixture was filtered over celite and the filter cake was washed with 30 ml of ethanol. The solvent was removed *in vacuo* to give **5** 2 H_2O as yellow oil in a quantitative yield.

^{1}H-NMR (400 MHz, $CDCl_3$) δ 7.42–7.26 (m, 5H), 5.96 (s, 1H), 4.32–4.10 (m, 2H), 3.76–3.65 (m, 2H), 3.37 (s, 3H), 3.06–2.95 (m, 1H), 2.76–2.62 (m, 1H).

Step d): MPDP+ bromide **6** (20). The suspension of **5** 2 H_2O (2.51 g, 11.01 mmol) in 90 ml dichloromethane (DCM) was cooled to 0°C and trifluoroacetic anhydride (4.49 g; 21.38 mmol) was added dropwise within 20 min. It was stirred at 0°C for 2 h, followed by the addition of 48% aq HBr (2.06 g, 12.23 mmol). The mixture was evaporated to dryness under reduced pressure at room temperature. The resulting crude product was recrystallized from acetone to yield 53% **6** (1.48 g, 5.87 mmol) as a yellow hygroscopic solid.

^{1}H-NMR (400 MHz, $CDCl_3$) δ 9.23 (d, J = 4.1 Hz, 1H), 7.69–7.60 (m, 2H), 7.52–7.40 (m, 3H), 6.89 (d, J = 4.6 Hz, 1H), 4.14 (t, J = 9.4 Hz, 2H), 3.93 (s, 3H), 3.32 (t, J = 9.4 Hz, 2H).

^{1}H-NMR (600 MHz, D_2O) δ 8.38 (d, J = 4.8 Hz, 1H), 7.82 (d, J = 7.9 Hz, 2H), 7.63–7.54 (m, 3H), 6.90 (d, J = 5.0 Hz, 1H), 4.04 (t, J = 10.1 Hz, 2H), 3.69 (s, 3H), 3.28 (t, J = 10.1 Hz, 2H).

^{13}C-NMR (101 MHz, $CDCl_3$) δ 164.1, 158.0, 134.5, 133.0, 129.5, 127.3, 113.9, 49.0, 47.7, 25.6.

^{13}C-NMR (150 MHz, D_2O) δ 163.5, 158.8, 134.6, 132.5, 129.0, 126.7, 112.9, 47.6, 46.0, 24.5.

HRMS (ESI, positive ion mode): [M]; calculated $C_{12}H_{14}N^+$: 172.1121 m/z; measured: 172.1124 m/z.

Analysis of 1-methyl-4-phenylpyridinium iodide (MPP^+ I^-) (Sigma-Aldrich)

^{1}H-NMR (400 MHz, DMSO) δ 9.02 (d, J = 6.9 Hz, 2H), 8.51 (d, J = 7.0 Hz, 2H), 8.11–8.04 (m, 2H), 7.70–7.61 (m, 3H), 4.34 (s, 3H).

^{1}H-NMR (600 MHz, D_2O) δ 8.74 (d, $J = 6.7$ Hz, 2H), 8.28 (d, $J = 6.7$ Hz, 2H), 7.97–7.92 (m, 2H), 7.70–7.62 (m, 3H), 4.36 (s, 3H).

^{13}C-NMR (101 MHz, DMSO) δ 154.3, 145.6, 133.5, 132.0, 129.7, 128.0, 124.1, 47.1.

^{13}C-NMR (150 MHz, D_2O) δ 156.3, 144.8, 133.8, 131.9, 129.5, 127.7, 124.6, 46.9.

HRMS (ESI, positive ion mode): [M]; calculated $C_{12}H_{12}N^{+}$: 170.0964 m/z; measured: 170.0968 m/z.

LUHMES cell culture

Methods for the generation, handling, and properties of LUHMES cells have been described in detail previously (47, 48). The cells were grown in standard conditions (serum-free) at a density of 300,000 cells per well in 24-well plates. The cells were derived from human fetal mesencephalon and were conditionally immortalized by expression of v-myc under a tet-off promoter. Upon addition of tetracycline, LUHMES cells differentiate within 5 days to fully post-mitotic human dopaminergic neurons with neurites of up to 1000 μm length (48). At this stage, the cells express highly active DATs and are susceptible to low micromolar levels of MPP^{+} (47, 48). For uptake experiments, cells were differentiated for 6 days and plated at a density of 300,000 cells/well in 24-well plates.

IMA 2.1 astrocytes

Generation and properties of the IMA cell line have recently been described in detail (45). These IMAs were cultured at 37°C (5% CO_2) in DMEM (normal glucose) (GIBCO) with 10% FCS (fetal calf serum from PAA) and 1% penicillin/streptomycin (10,000 U/ml stock). The cells were passaged by trypsinization for 2 min with 0.5% trypsin/DMEM every 2–3 days and reseeded at a ratio of 1:5 or 1:10. Experiments were performed 2 days after cells reached confluency in DMEM containing 10% FCS.

Overexpression of OCT3 and DAT

Gene contracts for human solute carrier family 6, member 3 (*DAT*), and sls22a solute carrier family 22, member 3 (*OCT3*), were purchased from SourceBioscience (Berlin, Germany). Both were obtained as inserts in the polymerase chain reaction vector (Invitrogen, Life Technologies Corporation) as clone number IRCBp5005O019Q (40147025- IMAGE ID) and clone number IRCKp5014K038Q (8860680- IMAGE ID), respectively. The *DAT* gene was cloned into the phsCtR2AU-W expression construct. This HIV-based vector was used as a plasmid to transfect the IMA cell line using Lipofectamine (Invitrogen, Life Technologies, Darmstadt, Germany). In this construct, the *DAT* gene was fused to the 3′ end of the tR2AU cassette (turbo red fluorescent protein from *Entacmaea quadricolor*, the 2A sequence of porcine teschovirus, and human ubiquitin sequences). Translation of this gene produces free tRFP protein by ribosomal skipping at the 2A site and free DAT protein by the action of cellular hydrolases, which cut at the 3′ end of the ubiquitin peptide. Cells that were successfully transfected and expressed the *DAT* gene could therefore be identified by their expression of red fluorescence. Cells were assayed 3 days after transfection.

The gene for *OCT3* was cloned into the pBIGFP vector. This construct contains a bidirectional inducible promoter allowing the expression of any gene cloned therein and the simultaneous expression of the linked marker gene eGFP (enhanced green fluorescent protein). Induction levels can be monitored by examination of eGFP intensities. Cells were transfected using Lipofectamine (Invitrogen, Life Technologies Corporation, Darmstadt, Germany) and subsequently selected with 200 μg/ml G418 for 10 days.

Immunostaining

Cells were grown in 24-well, plastic cell culture plates (Nunclon™). Following treatment, cells were fixed with 4% paraformaldehyde (PFA) for 20 min at 37°C and washed with phosphate-buffered saline (PBS). After blocking with 1% bovine serum albumin (Calbiochem, San Diego, CA) for 1 h, the primary antibody (anti-β-III-tubulin, Convance, mouse 1:1000) was added in PBS-Tween (0.1%) and the cells were incubated at 4°C overnight. Secondary antibody (anti-rat IgG-Alexa 488, Invitrogen, Darmstadt, Germany) was added for 45 min at RT. For visualization, an Olympus IX 81 microscope (Hamburg, Germany) equipped with an F-view CCD camera was used. Images were processed by Cell P software (Olympus).

Cell viability

Resazurin (Sigma-Aldrich) was added to the cell culture medium at a final concentration of 5 μg/ml and incubated at 37°C for at least 30 min. The fluorescence intensity was measured at 530 nm_{ex} and 590 nm_{em} with a Tecan Infinite M200 reader. Cell viability (in %) was calculated by normalizing the fluorescence values to the values obtained from untreated controls.

ATP assay

Cells grown in 24-well plates were lysed in PBS buffer containing 0.5% phosphatase inhibitor cocktail 2 (Sigma-Aldrich) and boiled at 95°C for 10 min. Following centrifugation at 10,000 *g* for 5 min to remove cell debris, protein content in the supernatant was measured and samples were adjusted to have equal concentrations. Samples were then diluted 1:10 in PBS/0.5% phosphatase inhibitor buffer. For the detection of ATP levels, a commercially available ATP assay reaction mixture (Sigma-Aldrich) containing luciferin and luciferase was used (50 μl of adjusted sample plus 100 μl of assay mix was added to a black 96-well plate). Standards were prepared by serial dilutions of ATP disodium salt hydrate (Sigma-Aldrich) to obtain concentrations ranging from 1000 to 7.8 nM.

Vesicle uptake assay

For vesicle preparation, stock solutions of 100 mg/ml DOPC (1,2-dioleoyl-sn-glycero-3-phosphocholine) and 100 mg/ml DOPE (1,2-dioleoyl-sn-glycero-3-phosphoethanolamine) (Avanti) in $CHCl_3$ were prepared. For the production of a 2 ml vesicle suspension, 102 μl of DOPC and 98 μl of DOPE stock solutions were mixed in a glass tube and evaporated for 30 min under vacuum while rotating to remove $CHCl_3$. The lipid film was then resuspended in 1 ml of 20% Triton X-100 in PBS, and air was removed by N_2 degassing. The mixture under N_2 atmosphere was then briefly sonicated in a water bath and

allowed to rest at room temperature until a clear solution was observed, indicating complete solubilization of the lipids. To remove the detergent, 600 mg Bio-Beads SM-2 (Bio-Rad) pre-equilibrated in PBS were added to the clear lipid/detergent mixture diluted 1:1 in PBS and incubated at 4°C on a rotator for 16 h. For removal of the beads, the vesicle suspension was collected with capillary tips and transferred to a separate tube. For uptake assays, the vesicle suspension (10 mg lipids/ml) in PBS was incubated with MPP$^+$ or MPDP$^+$ for 2 h at 37°C. To remove free MPP$^+$/MPDP$^+$, vesicles were separated by loading 100 μl of the sample onto an NAP™-5 Sephadex™ G-25 column and a stepwise addition of 250 μl volumes of PBS for elution. As control, vesicle-free solutions containing MPP$^+$ or MPDP were added. The vesicle-containing fractions were analyzed separately, and MPP$^+$ or MPDP$^+$ values in the vesicle fractions were integrated.

Erythrocyte uptake assay

Human blood was collected in EDTA (1.6 mg/ml blood)-containing tubes (Sarstedt S-Monovette, Nuembrecht, Germany) and centrifuged at 200 *g* for 4 min. The erythrocyte fraction was resuspended in a buffer containing 21 mM Tris, 4.7 mM KCl, 2 mM $CaCl_2$, 140 mM NaCl, 1.2 mM $MgSO_4$, and 5.5 mM glucose, pH 7.4. The cells were washed twice with the buffer by centrifugation at 1000 *g* for 1 min. The cells were then treated with MPP$^+$ or MPDP$^+$, as indicated. To assess intracellular MPP$^+$ levels, the erythrocytes were again washed by three consecutive centrifugation steps (1000 *g*, 1 min) to remove extracellular MPP$^+$ or MPDP$^+$. The erythrocytes were then lysed by resuspension in H_2O for 20 min, supported by moderate sonication. Proteins were precipitated by the addition of 0.4 M perchloric acid, and the supernatant was filtered through a 0.22 μm membrane and analyzed by high performance liquid chromatography (HPLC).

MPTP conversion in the brain

C57BL/6JRj male mice were kept under 12 h light/12 h dark cycles at a temperature of 23°C and 55% humidity. The animals had *ad libitum* access to food and water. All animal studies were approved by the appropriate institutional governmental agency (Regierungspraesidium Tuebingen, Germany) and carried out in an Association for Assessment and Accreditation of Laboratory Animal Care International-accredited facility in accordance with the European Convention for Animal Care and Use of Laboratory Animals. The mice were intraperitoneally injected with MPTP (30 mg/kg; free base in 0.9% NaCl), cared for over the time intervals indicated, and then killed by cervical dislocation. The striatum and cerebellum of each mouse were dissected after decapitation. The tissues were homogenized in 1 ml of 0.4 M perchloric acid by sonication. Following a centrifugation step at 2000 *g* for 10 min at 4°C, the pellet was resuspended in 250 μM of 1 M NaOH. Total protein content was detected by a BCA assay kit. The supernatant was filtered through a 0.22 μm membrane and analyzed by HPLC.

HPLC analysis

Detection of MPTP, MPP$^+$, and MPDP$^+$ was performed on a Kontron system (Goebel Analytic, Au/Hallertau, Germany) comprising a model 520 pump, model 560 autosampler, and models 535 and 430 diode array detectors set at 245 nm for MPTP, 295 nm for MPP$^+$, and 345 nm for MPDP$^+$. Samples were acidified with 9 μl perchloric acid (70%) per ml volume of sample and centrifuged at 10,000 *g* for 15 min. The supernatant was filtered through a Chromafil PET-20/15MS filter with 0.2 μm pore size from Macherey Nagel (Düren, Germany). Separation was carried out on a C18 nucleosil column (250 × 4.6 mm; 5 μm particle size) from Macherey Nagel (Düren, Germany) at room temperature. The mobile phase consisted of acetonitrile: distilled water: triethylamine: sulfuric acid (12.50: 86.18: 1.04: 0.28, v/v, pH 2.3). The mobile phase was degassed with an online vacuum degasser and delivered isocratically at a flow rate of 1 ml/min at an average pressure of 145 bar. Data analysis was performed with Geminyx II software (Goebel Analytic). Peak areas of MPTP, MPDP$^+$, and MPP$^+$ were evaluated with the Geminyx II software by the application of standard curves obtained for each of the three individual compounds.

Detection of ^{13}C-labeled intracellular metabolites

For stable isotope labeling, cells were incubated with [U-$^{13}C_6$] glucose for at least 18 h. To infer relative intracellular fluxes, intracellular metabolites were extracted and measured with GC/MS. Cells grown in six-well plates were washed with 1 ml saline solution (0.9%) and quenched with 0.4 ml of cold (–20°C) methanol. After adding an equal volume of cold water, cells were collected with a cell scraper and transferred in tubes containing 0.4 ml of cold (–20°C) chloroform. The extracts were shaken at 1400 rpm for 20 min at 4°C and centrifuged at 16,000 *g* for 5 min at 4°C; 0.3 ml of the upper aqueous phase was collected in specific GC glass vials and evaporated under vacuum at –4°C using a refrigerated CentriVap Concentrator (Labconco). Metabolite derivatization was performed using an Agilent autosampler. Dried polar metabolites were dissolved in 15 μl of 2% methoxyamine hydrochloride in pyridine at 45°C. After 60 min, an equal volume of 2,2,2-trifluoro-N-methyl-N-trimethylsilyl-acetamide +1% chloro-trimethyl-silane was added and metabolites were incubated for 30 min at 45°C.

GC/MS analysis was performed using an Agilent 6890GC equipped with a 30 m DB-35MS capillary column. The GC was connected to an Agilent 5975C MS operating under electron impact ionization at 70 eV. The MS source was held at 230°C and the quadrupole at 150°C. The detector was operated in scan mode and 1 μl of derivatized sample was injected in splitless mode. Helium was used as a carrier gas at a flow rate of 1 ml/min. The GC oven temperature was held at 80°C for 6 min and increased to 300°C at a rate of 6°C/min. After 10 min, the temperature was increased to 325°C at a rate of 10°C/min for 4 min. The run time for each sample was 59 min. For determination of the mass isotopomer distribution (MID) of citrate, the mass spectrum was corrected for natural isotope abundance. Data processing from raw spectra to MID correction and determination was performed using MetaboliteDetector software (24).

Acknowledgments

This work was supported by RTG 1331, BMBF, the Doerenkamp-Zbinden-Foundation, KoRS-Chemical Biology, and the Collaborative Research Center 969 ''Chemical and Biological Principles of Cellular Proteostasis,'' funded by the Deutsche Forschungsgemeinschaft.

Author Disclosure Statement

No competing financial interests exist.

References

1. Bajpai P, Sangar MC, Singh S, Tang W, Bansal S, Chowdhury G, Cheng Q, Fang JK, Martin MV, Guengerich FP, and Avadhani NG. Metabolism of 1-methyl-4-phenyl-1,2,3,6-tetrahydropyridine by mitochondrion-targeted cytochrome P450 2D6: implications in Parkinson disease. *J Biol Chem* 288: 4436–4451, 2013.
2. Barzilai A, Daily D, Zilkha-Falb R, Ziv I, Offen D, Melamed E, and Shirvan A. The molecular mechanisms of dopamine toxicity. *Adv Neurol* 91: 73–82, 2003.
3. Beal MF. Experimental models of Parkinson's disease. *Nat Rev Neurosci* 2: 325–334, 2001.
4. Castagnoli N, Chiba K, and Trevor AJ. Potential bioactivation pathways for the neurotoxin 1-methyl-4-phenyl-1,2,3,6-tetrahydropyridine (MPTP). *Life Sci* 36: 225–230, 1985.
5. Chiba K, Peterson LA, Castagnoli KP, Trevor AJ, and Castagnoli N. Studies on the molecular mechanism of bioactivation of the selective nigrostriatal toxin 1-methyl-4-phenyl-1,2,3,6-tetrahydropyridine. *Drug Metab Dispos* 13: 342–347, 1985.
6. Chiba K, Trevor A, and Castagnoli N. Metabolism of the neurotoxic tertiary amine, MPTP, by brain monoamine oxidase. *Biochem Biophys Res Commun* 120: 574–578, 1984.
7. Choi WS, Kruse SE, Palmiter RD, and Xia Z. Mitochondrial complex I inhibition is not required for dopaminergic neuron death induced by rotenone, MPP+, or paraquat. *Proc Natl Acad Sci USA* 105: 15136–15141, 2008.
8. Cobuzzi RJ, Neafsey EJ, and Collins MA. Differential cytotoxicities of N-methyl-beta-carbolinium analogues of MPP+ in PC12 cells: insights into potential neurotoxicants in Parkinson's disease. *J Neurochem* 62: 1503–1510, 1994.
9. Cui M, Aras R, Christian WV, Rappold PM, Hatwar M, Panza J, Jackson-Lewis V, Javitch JA, Ballatori N, Przedborski S, and Tieu K. The organic cation transporter-3 is a pivotal modulator of neurodegeneration in the nigrostriatal dopaminergic pathway. *Proc Natl Acad Sci USA* 106: 8043–8048, 2009.
10. Dauer W and Przedborski S. Parkinson's disease: mechanisms and models. *Neuron* 39: 889–909, 2003.
11. Devos D, Moreau C, Devedjian JC, Kluza J, Petrault M, Laloux C, Jonneaux A, Ryckewaert G, Garçon G, Rouaix N, Duhamel A, Jissendi P, Dujardin K, Auger F, Ravasi L, Hopes L, Grolez G, Firdaus W, Sablonnière B, Strubi-Vuillaume I, Zahr N, Destée A, Corvol JC, Pöltl D, Leist M, Rose C, Defebvre L, Marchetti P, Cabantchik ZI, and Bordet R. Targeting chelatable iron as a therapeutic modality in Parkinson's disease. *Antioxid Redox Signal*. 21: 195–210, 2014.
12. Dexter DT, Wells FR, Agid F, Agid Y, Lees AJ, Jenner P, and Marsden CD. Increased nigral iron content in postmortem parkinsonian brain. *Lancet* 2: 1219–1220, 1987.
13. Di Monte DA, Schipper HM, Hetts S, and Langston JW. Iron-mediated bioactivation of 1-methyl-4-phenyl-1,2,3,6-tetrahydropyridine (MPTP) in glial cultures. *Glia* 15: 203–206, 1995.
14. Di Monte DA, Wu EY, Delanney LE, Irwin I, and Langston JW. Toxicity of 1-methyl-4-phenyl-1,2,3,6-tetrahydropyridine in primary cultures of mouse astrocytes. *J Pharmacol Exp Ther* 261: 44–49, 1992.
15. Di Monte DA, Wu EY, Irwin I, Delanney LE, and Langston JW. Biotransformation of 1-methyl-4-phenyl-1,2,3,6-tetrahydropyridine in primary cultures of mouse astrocytes. *J Pharmacol Exp Ther* 258: 594–600, 1991.
16. Di Monte DA, Wu EY, Irwin I, Delanney LE, and Langston JW. Production and disposition of 1-methyl-4-phenylpyridinium in primary cultures of mouse astrocytes. *Glia* 5: 48–55, 1992.
17. Dmitriev RI, Zhdanov AV, Jasionek G, and Papkovsky DB. Assessment of cellular oxygen gradients with a panel of phosphorescent oxygen-sensitive probes. *Anal Chem* 84: 2930–2938, 2012.
18. Fries DS de Vries J, Hazelhoff B, and Horn AS. Synthesis and toxicity toward nigrostriatal dopamine neurons of 1-methyl-4-phenyl-1,2,3,6-tetrahydropyridine (MPTP) analogues. *J Med Chem* 29: 424–427, 1986.
19. Fuller RW, Hemrick-Luecke SK, and Perry KW. Tissue concentrations of MPTP and MPP+ in relation to catecholamine depletion after the oral or subcutaneous administration of MPTP to mice. *Life Sci* 45: 2077–2083, 1989.
20. Gessner W, Brossi A, Shen RS, Fritz RR, and Abell CW. Conversion of 1-methyl-4-phenyl-1,2,3,6-tetrahydropyridine (mptp) and its 5-methyl analog into pyridinium salts. *Helv Chim Acta* 67: 2037–2042, 1984.
21. Giovanni A, Sieber BA, Heikkila RE, and Sonsalla PK. Studies on species sensitivity to the dopaminergic neurotoxin 1-methyl-4-phenyl-1,2,3,6-tetrahydropyridine. Part 1: systemic administration. *J Pharmacol Exp Ther* 270: 1000–1007, 1994.
22. Glube N and Langguth P. Caki-1 cells as a model system for the interaction of renally secreted drugs with OCT3. *Nephron Physiol* 108: 18–28, 2008.
23. Heikkila RE, Manzino L, Cabbat, FS, and Duvoisin RC. Protection against the dopaminergic neurotoxicity of 1-methyl-4-phenyl-1,2,5,6-tetrahydropyridine by monoamine oxidase inhibitors. *Nature* 311: 467–469, 1984.
24. Hiller K, Hangebrauk J, Jäger C, Spura J, Schreiber K, and Schomburg D. MetaboliteDetector: comprehensive analysis tool for targeted and nontargeted GC/MS based metabolome analysis. *Anal Chem* 81: 3429–3439, 2009.
25. Jackson-Lewis V, Blesa J, and Przedborski S. Animal models of Parkinson's disease. *Parkinsonism Relat Disord* 18 Suppl 1: S183–S185, 2012.
26. Javitch JA, D'Amato RJ, Strittmatter SM, and Snyder SH. Parkinsonism-inducing neurotoxin, N-methyl-4-phenyl-1,2,3,6-tetrahydropyridine: uptake of the metabolite N-methyl-4-phenylpyridine by dopamine neurons explains selective toxicity. *Proc Natl Acad Sci U S A* 82: 2173–2177, 1985.
27. Jones DP. Intracellular diffusion gradients of O2 and ATP. *Am J Physiol* 250: C663–C675, 1986.
28. Kadar H, Le Douaron G, Amar M, Ferrié L, Figadère B, Touboul D, Brunelle A, and Raisman-Vozari R. MALDI mass spectrometry imaging of 1-methyl-4-phenylpyridinium (MPP+) in mouse brain. *Neurotox Res* 25: 135–145, 2014.
29. Kaur D, Yantiri F, Rajagopalan S, Kumar J, Mo JQ, Boonplueang R, Viswanath V, Jacobs R, Yang L, Beal MF, DiMonte D, Volitaskis I, Ellerby L, Cherny RA, Bush AI, and Andersen JK. Genetic or pharmacological iron chelation prevents MPTP-induced neurotoxicity in vivo: a novel therapy for Parkinson's disease. *Neuron* 37: 899–909, 2003.
30. Korytowski W, Felix CC, and Kalyanaraman B. Mechanism of oxidation of 1-methyl-4-phenyl-2,3-dihydropyridinium (MPDP+). *Biochem Biophys Res Commun* 144: 692–698, 1987.
31. Langston JW, Ballard P, Tetrud JW, and Irwin I. Chronic Parkinsonism in humans due to a product of meperidine-analog synthesis. *Science* 219: 979–980, 1983.

32. Langston JW, Irwin I, Langston EB, and Forno LS. Pargyline prevents MPTP-induced parkinsonism in primates. *Science* 225: 1480–1482, 1984.
33. Lin CJ, Tai Y, Huang MT, Tsai YF, Hsu HJ, Tzen KY, and Liou HH. Cellular localization of the organic cation transporters, OCT1 and OCT2, in brain microvessel endothelial cells and its implication for MPTP transport across the blood-brain barrier and MPTP-induced dopaminergic toxicity in rodents. *J Neurochem* 114: 717–727, 2010.
34. Lugo-Huitrón R, Ugalde Muñiz P, Pineda B, Pedraza-Chaverrí J, Ríos C, and Pérez-de la Cruz V. Quinolinic acid: an endogenous neurotoxin with multiple targets. *Oxid Med Cell Longev* 2013: 104024, 2013.
35. Meiser J, Weindl D, and Hiller K. Complexity of dopamine metabolism. *Cell Commun Signal* 11: 34, 2013.
36. Mik EG, Stap J, Sinaasappel M, Beek JF, Aten JA, van Leeuwen TG, and Ince C. Mitochondrial PO2 measured by delayed fluorescence of endogenous protoporphyrin IX. *Nat Methods* 3: 939–945, 2006.
37. Naganuma F, Yoshikawa T, Nakamura T, Iida T, Harada R, Mohsen AS, Miura Y, and Yanai K. Predominant role of plasma membrane monoamine transporters in monoamine transport in 1321N1, a human astrocytoma-derived cell line. *J Neurochem* 129: 591–601, 2014.
38. Nicklas WJ, Vyas I, and Heikkila RE. Inhibition of NADH-linked oxidation in brain mitochondria by 1-methyl-4-phenyl-pyridine, a metabolite of the neurotoxin, 1-methyl-4-phenyl-1,2,5,6-tetrahydropyridine. *Life Sci* 36: 2503–2508, 1985.
39. Peterson LA, Caldera PS, Trevor A, Chiba K, and Castagnoli N. Studies on the 1-methyl-4-phenyl-2,3-dihydropyridinium species 2,3-MPDP+, the monoamine oxidase catalyzed oxidation product of the nigrostriatal toxin 1-methyl-4-phenyl-1,2,3,6-tetrahydropyridine (MPTP). *J Med Chem* 28: 1432–1436, 1985.
40. Ramsay RR, Dadgar J, Trevor A, and Singer TP. Energy-driven uptake of N-methyl-4-phenylpyridine by brain mitochondria mediates the neurotoxicity of MPTP. *Life Sci* 39: 581–588, 1986.
41. Ramsay RR, and Singer TP. Energy-dependent uptake of N-methyl-4-phenylpyridinium, the neurotoxic metabolite of 1-methyl-4-phenyl-1,2,3,6-tetrahydropyridine, by mitochondria. *J Biol Chem* 261: 7585–7587, 1986.
42. Rappold PM, Cui M, Chesser AS, Tibbett J, Grima JC, Duan L, Sen N, Javitch JA, and Tieu K. Paraquat neurotoxicity is mediated by the dopamine transporter and organic cation transporter-3. *Proc Natl Acad Sci U S A* 108: 20766–20771, 2011.
43. Reinhard JF, Jr., Diliberto EJ, Jr., Viveros OH, and Daniels AJ. Subcellular compartmentalization of 1-methyl-4-phenylpyridinium with catecholamines in adrenal medullary chromaffin vesicles may explain the lack of toxicity to adrenal chromaffin cells. *Proc Natl Acad Sci U S A* 84: 8160–8164, 1987.
44. Russell SM, Davey J, and Mayer RJ. The vectorial orientation of human monoamine oxidase in the mitochondrial outer membrane. *Biochem J* 181: 7–14, 1979.
45. Schildknecht S, Kirner S, Henn A, Gasparic K, Pape R, Efremova L, Maier O, Fischer R, and Leist M. Characterization of mouse cell line IMA 2.1 as a potential model system to study astrocyte functions. *ALTEX* 29: 261–274, 2012.
46. Schildknecht S, Pape R, Müller N, Robotta M, Marquardt A, Bürkle A, Drescher M, and Leist M. Neuroprotection by minocycline caused by direct and specific scavenging of peroxynitrite. *J Biol Chem* 286: 4991–5002, 2011.
47. Schildknecht S, Pöltl D, Nagel DM, Matt F, Scholz D, Lotharius J, Schmieg N, Salvo-Vargas A, and Leist M. Requirement of a dopaminergic neuronal phenotype for toxicity of low concentrations of 1-methyl-4-phenylpyridinium to human cells. *Toxicol Appl Pharmacol* 241: 23–35, 2009.
48. Scholz D, Pöltl D, Genewsky A, Weng M, Waldmann T, Schildknecht S, and Leist M. Rapid, complete and large-scale generation of post-mitotic neurons from the human LUHMES cell line. *J Neurochem* 119: 957–971, 2011.
49. Shang T, Uihlein AV, Van Asten J, Kalyanaraman B, and Hillard CJ. 1-Methyl-4-phenylpyridinium accumulates in cerebellar granule neurons via organic cation transporter 3. *J Neurochem* 85: 358–367, 2003.
50. Sulzer D, Bogulavsky J, Larsen KE, Behr G, Karatekin E, Kleinman MH, Turro N, Krantz D, Edwards RH, Greene LA, and Zecca L. Neuromelanin biosynthesis is driven by excess cytosolic catecholamines not accumulated by synaptic vesicles. *Proc Natl Acad Sci U S A* 97: 11869–11874, 2000.
51. Takahashi E and Doi K. Impact of diffusional oxygen transport on oxidative metabolism in the heart. *Jpn J Physiol.* 48: 243–252, 1998.
52. Trevor AJ, Castagnoli N, and Singer TP. The formation of reactive intermediates in the MAO-catalyzed oxidation of the nigrostriatal toxin 1-methyl-4-phenyl-1,2,3,6-tetrahydropyridine (MPTP). *Toxicology* 49: 513–519, 1988.
53. Tribl F, Asan E, Arzberger T, Tatschner T, Langenfeld E, Meyer HE, Bringmann G, Riederer P, Gerlach M, and Marcus K. Identification of L-ferritin in neuromelanin granules of the human substantia nigra: a targeted proteomics approach. *Mol Cell Proteomics* 8: 1832–1838, 2009.
54. Uhl GR, Javitch JA, and Snyder SH. Normal MPTP binding in parkinsonian substantial nigra: evidence for extraneuronal toxin conversion in human brain. *Lancet* 1: 956–957, 1985.
55. Wu EY, Langston JW, and Di Monte DA. Toxicity of the 1-methyl-4-phenyl-2,3-dihydropyridinium and 1-methyl-4-phenylpyridinium species in primary cultures of mouse astrocytes. *J Pharmacol Exp Ther* 262: 225–230, 1992.
56. Zucca FA, Basso E, Cupaioli FA, Ferrari E, Sulzer D, Casella L, and Zecca L. Neuromelanin of the human substantia nigra: an update. *Neurotox Res* 25: 13–23, 2014.

Address correspondence to:
Dr. Stefan Schildknecht
Department of Biology
University of Konstanz
PO Box M657
Universitätsstr. 10
Konstanz 78457
Germany

E-mail: stefan.schildknecht@uni-konstanz.de

Date of first submission to ARS Central, May 23, 2015; date of final revised submission, September 13, 2015; date of acceptance, September 14, 2015.

Abbreviations Used

1,2-MPDP = 1-methyl-4-phenyl-1,2-dihydropyridine
DA = dopamine
DAT = dopamine transporter
DOPC = 1,2-dioleoyl-*sn*-glycero-3-phosphatidylcholine
DOPE = 1,2-dioleoyl-*sn*-glycero-3-phosphoethanolamine
HRMS = high-resolution mass spectrometry
IMA = immortalized mouse astrocytes
LUHMES = lund human mesencephalic neuron
MAO = monoamine oxidase
MID = mass isotopomer distribution
$MPDP^+$ = 1-methyl-4-phenyl-2,3-dihydropyridinium
MPP^+ = 1-methyl-4-phenyl-pyridinium
MPTP = 1-methyl-4-phenyl-tetrahydropyridine
OCT = organic cation transporter
PBS = phosphate-buffered saline
ROS = reactive oxygen species
SD = standard deviation
TCA = tricarboxylic acid
TFAA = trifluoroacetic anhydride
THF = tetrahydrofuran